Available online at www.sciencedirect.com
ScienceDirect
Journal of the European Ceramic Society 28 (2008) 1287–1296
www.elsevier.com/locate/jeurceramsoc

Spark plasma sintering of Zr- and Hf-borides with decreasing amounts of $MoSi_2$ as sintering aid

D. Sciti [a,*], L. Silvestroni [a], M. Nygren [b]

[a] *ISTEC-CNR, Institute for Science and Technology of Ceramics, Via Granarolo 64, I-48018 Faenza, Italy*
[b] *Department of Inorganic Chemistry, Arrhenius Laboratory, Stockolm University, SE-10691 Stockolm, Sweden*

Received 26 May 2007; received in revised form 17 September 2007; accepted 30 September 2007
Available online 26 November 2007

Abstract

ZrB_2- and HfB_2-based composites containing 1, 3, and 9 vol.% $MoSi_2$ as sintering aid were densified by spark plasma sintering at temperatures ranging from 1700 to 1950 °C, with an applied pressure of 100 MPa. As received ZrB_2 and HfB_2 powders were also sintered at temperatures in the range of 2100–2200 °C. Fully dense samples were obtained between 1750 and 1850 °C when $MoSi_2$ was added. As received ZrB_2 powder was sintered to 98% at 2100 °C. The microstructural features were investigated by means of SEM–EDS technique. Silicon carbide was detected in all the doped compositions along with significant amounts of oxide species (Hf/ZrO_2 and SiO_2). Vickers hardness and fracture toughness were measured by indentation technique on polished sections. The effect of the $MoSi_2$ content on densification, microstructure and mechanical properties is discussed.

Keywords: Spark plasma sintering; Borides; Microstructure; HfB_2; ZrB_2; $MoSi_2$

1. Introduction

Spark plasma sintering (SPS) belongs to a class of technologies that employ a pulsed dc current to activate and improve sintering kinetics.[1–8] In nearly all the investigations on spark plasma sintering/field assisted sintering, higher heating rates, lower sintering temperatures and shorter dwelling times have been used in comparison with those attained in conventional sintering techniques (hot pressing, pressureless sintering, etc.). Higher densities, refined microstructures, clean grain boundaries and elimination of surface impurities have been reported for several ceramic materials densified by field assisted sintering, as well as an overall improvement in the materials performance.[1–8] In view of the potential offered by this technique, this work deals with spark plasma sintering of the so-called ultra-high-temperature ceramics (UHTC), namely borides of zirconium and hafnium, which are notorious for their poor sinterability. The interest in these compounds derives from the fact that they possess several desired engineering properties such as high melting points (>3200 °C), solid-state stability and good thermo-chemical and thermo-mechanical properties. Applications such as leading edges and nose caps in hypersonic re-entry space vehicles, rocket nozzle inserts and air-augmented propulsion system components are forecast in the aerospace industry.[9–14] Due to the high melting point and low self-diffusion coefficient, the sintering of Hf- and Zr-borides needs pressure-assisted sintering procedures at temperatures of the order of 2000 °C or even higher.[13–17] Attempts to consolidate ZrB_2 by pressureless sintering at temperature <2100 °C have shown that a non-densifying vapour phase transport mechanism is dominant for this compound, leading to a coarsening of the microstructure that in turn leads to a reduction of the driving force for sintering.[18] Moreover, the unavoidable presence of surface oxides, such as B_2O_3 and HfO_2/ZrO_2 is an additional factor which hinders the densification of Hf/ZrB_2 compounds. One promising approach for overcoming these problems is the use of rapid heating rates through temperature regimes where grain coarsening occurs. From this point of view, field-assisted sintering offers the opportunity of extremely high heating rates. Furthermore, it has also been reported that the application of an external field may lead to elimination of surface oxides by electrical discharge.[4,5] So far, few attempts have been made to densify

* Corresponding author. Tel.: +39 0546 699748; fax: +39 0546 46381.
E-mail address: dile@istec.cnr.it (D. Sciti).

0955-2219/$ – see front matter © 2007 Elsevier Ltd. All rights reserved.
doi:10.1016/j.jeurceramsoc.2007.09.043

these compounds by spark plasma sintering. HfB_2 and ZrB_2 with 15 vol.% $MoSi_2$ were densified to nearly full density at 1750 °C, whilst attempts to sinter as-received Hf- or Zr-borides powders led to very poor densification (about 70% of relative density) even at 2100–2200 °C.[19–22]

In this contribution, a deeper investigation of the effect of spark plasma sintering on the densification of these borides is carried out. The aim is to obtain fine-grained and dense materials with as low as possible amount of sintering aid in order to minimize the deleterious effects of secondary phases. $MoSi_2$ is selected as ceramic additive for Hf- and Zr-borides, as it has been shown that in amounts as high as 15–20 vol.% is effective for the densification using conventional sintering techniques.[20,21,23] In this work, the amount of sintering aid is progressively reduced, starting from a content of 9 vol.%, and finally the densification of HfB_2 and ZrB_2 without any additive is attempted. Densification behaviour and microstructural features are discussed. Preliminary mechanical tests (hardness and fracture toughness) are also performed on selected materials.

2. Experimental

Commercial powders (Table 1) were used to prepare the following compositions (vol.%):

$ZrB_2 + 9MoSi_2$ (ZB9); $HfB_2 + 9MoSi_2$ (HB9)

$ZrB_2 + 3MoSi_2$ (ZB3); $HfB_2 + 3MoSi_2$ (HB3)

$ZrB_2 + 1MoSi_2$ (ZB1); $HfB_2 + 1MoSi_2$ (HB1)

Undoped powders were also sintered, labelled as ZB0 and HB0. The powder mixtures were first ultrasonically treated and then ball-milled for 24 h in absolute ethanol using zirconia milling media, subsequently dried in a rotary evaporator and sieved through a 60-mesh screen size. For sintering tests on undoped powders, HfB_2 and ZrB_2 were ultrasonically treated to eliminate agglomerates and milled using zirconia milling media. Doped and undoped powders were sintered using a spark plasma sintering furnace in a graphite mould. A double layer of graphite blanket was placed around the die in order to minimize the heat loss. The temperature was measured by an optical pyrometer focused onto the graphite die. Various experiments based on temperature-induced sintering events suggest an experimental error of ±15 °C of the recorded temperature in the temperature region of 1800–2200 °C. The sintered pellets were 1.2 cm in diameter and 0.5 cm in height.

For $MoSi_2$-doped powders, the sintering cycle was adopted as follows. From room temperature (RT) to 600 °C the heating rate was set at 300 °C/min. At 600 °C, the pressure of 100 MPa was applied and the temperature was then raised from 600 to 1400 °C using a heating rate of 200 °C/min. From 1400 °C to the final sintering temperature (1700–1900 °C) the heating rate was decreased to 100 °C/min. Holding times at the maximum temperature were 3 or 5 min.

For undoped powders a slightly different heating cycle was adopted; from room temperature (RT) to 600 °C the heating rate was set to 300 °C/min. At 600 °C, a pressure of 75 MPa was applied for ZrB_2 (65 MPa for HfB_2) and the temperature was raised from 600 to 1600 °C using a heating rate of 200 °C/min and from 1600 °C to the maximum temperature at a rate of 100 °C/min. The holding time was 3–5 min.

Bulk densities were measured by the Archimedes method. Relative densities were determined as the ratio between bulk densities and theoretical densities calculated on the basis of the starting nominal compositions. Crystalline phases were identified by X-ray diffraction (Siemens D500, Karlsruhe, Germany). The microstructures were analysed using scanning electron microscopy (SEM, Cambridge S360, Cambridge, UK) and energy dispersive spectroscopy (EDS, INCA Energy 300, Oxford instruments, UK). The SEM–EDS studies were performed on samples sections that were cut from the sintered pellets containing the direction of applied pressure and then polished with diamond paste to 0.25 μm. Microstructural parameters were determined through image analysis on SEM micrographs of polished surfaces (Image Pro-plus 4.5.1, Media Cybernetics, Silver Springs, MD, USA).

Vickers microhardness (HV1.0) was measured with a load of 9.81 N, using a Zwick 3212 tester (Zwick, Ulm, Germany). Eight to 10 indentations were made for each sample. Fracture toughness (K_{Ic}) was evaluated by the direct crack measurement (DCM) using the equation of Evans and Charles.[24] Five indentations were performed for each sample.

3. Results and discussion

3.1. Densification behaviour and grain growth

Doped HfB_2 and ZrB_2 powders generally showed a good sinterability and their sintering behaviour indicated that they were fully dense or close to being fully dense after a permanence of 1–3 min at the maximum temperature. A typical densification curve is shown in Fig. 1, for the composition HB1, sintered at 1800 °C. All the relative density data are displayed in Fig. 2a and b, as a function of the sintering temperature and for different contents of $MoSi_2$. It must be pointed out that given sintering temperatures were the ones recorded on the surface of the graphite die and that the temperatures experienced by the

Table 1
Characteristics of the starting powders

	Supplier	Phase	Grade	Grain size range (μm)	Impurities (wt.%)
ZrB_2	H.C. Starck, Germany	Hexagonal	B	0.1–8	(Maximum content): C: 0.25, O: 2, N: 0.25, Fe: 0.1, Hf: 0.2
HfB_2	Cerac Inc., USA	Hexagonal	325 mesh	0.5–5	Zr: 0.47, Al: 0.07, Fe: 0.01
$MoSi_2$	Aldrich Chemicals	Tetragonal	<2 μm	0.1–3	O: 1–2

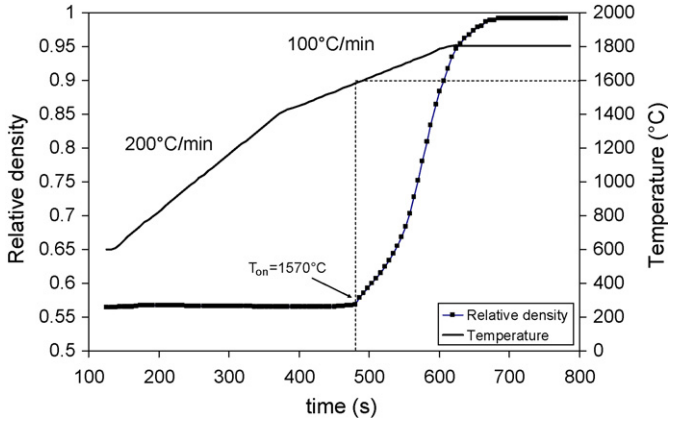

Fig. 1. Typical densification curve of composition $HfB_2 + 1MoSi_2$ (HB1) at 1800 °C. T_{on} = temperature at which densification starts.

samples were certainly higher. This point is further discussed below.

It can be noticed that for ZrB_2-based materials (Fig. 2a), specimens were all sintered to final densities higher than 95%. After decreasing the amount of sintering aid, increased sintering temperatures were necessary to obtain the same level of density. For 9 and 3% doping, 98% dense samples were obtained at 1700 and 1750 °C, respectively, whilst for 1% doping, the temperature had to be raised to 1850 °C. Undoped ZrB_2 was densified to 98% of relative density at 2100 °C.

For HfB_2-based compositions (Fig. 2b), the highest density values were achieved in the range of 1700–1800 °C. At 1750 °C, relative densities in excess of 95% were obtained irrespective of the $MoSi_2$ variation between 9 and 1 vol.%. For compositions containing 9 and 3 vol.% $MoSi_2$, an increase of final density was observed with increasing the sintering temperature. In contrast, from data displayed in Fig. 2b, it is apparent that for compositions with 1% doping, a decrease of the final density was observed when increasing the sintering temperature. It should be noted that the real solid density of either ZrB_2- or HfB_2-doped samples was higher due to presence of impurity phases of low densities, see below. Finally, attempts to densify undoped HfB_2 powders led to final densities of the order of 80%, even after increasing the sintering temperature to 2300 °C.

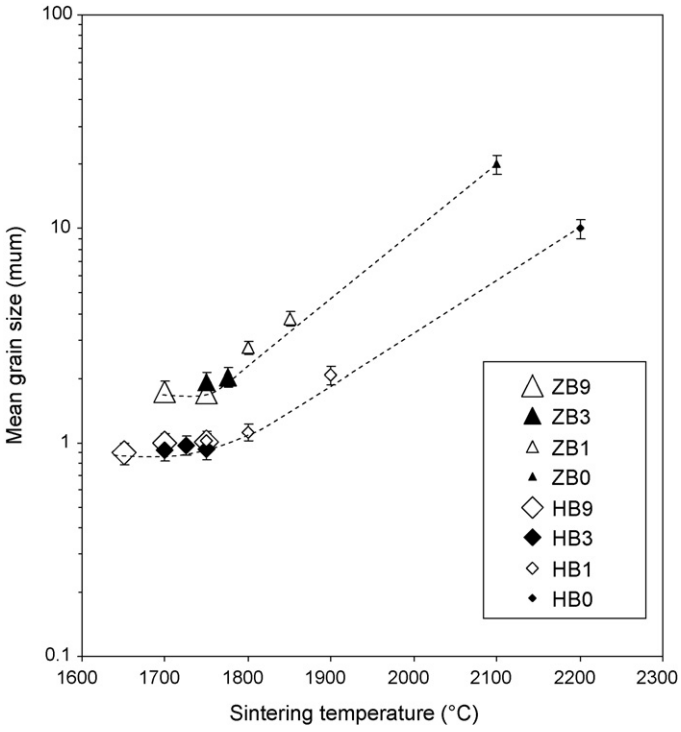

Fig. 3. Mean grain size as a function of the sintering temperature for different sintering aid contents. The dotted lines are eye guidelines.

Formation of droplets was noticed for compositions containing 9% of $MoSi_2$, more abundantly for ZrB_2 than for HfB_2-based compositions, which is consistent with liquid formation. No droplets were observed at temperature below or equal to 1700 °C.

The mean grain size of the boride grains is reported as a function of the sintering temperature in Fig. 3, including all the sintered compositions. Up to 1800 °C, the mean grain size was <2 μm for ZrB_2-based compositions and <1 μm for HfB_2 ones. However, the decrease of the sintering aid content from 3% and to 1% and the increase of the sintering temperature caused a notable coarsening of the microstructure, in both cases. The mean grain sizes of HfB_2-based compositions were smaller than those of the corresponding ZrB_2-based compositions, due to the fineness of the starting HfB_2 powder.

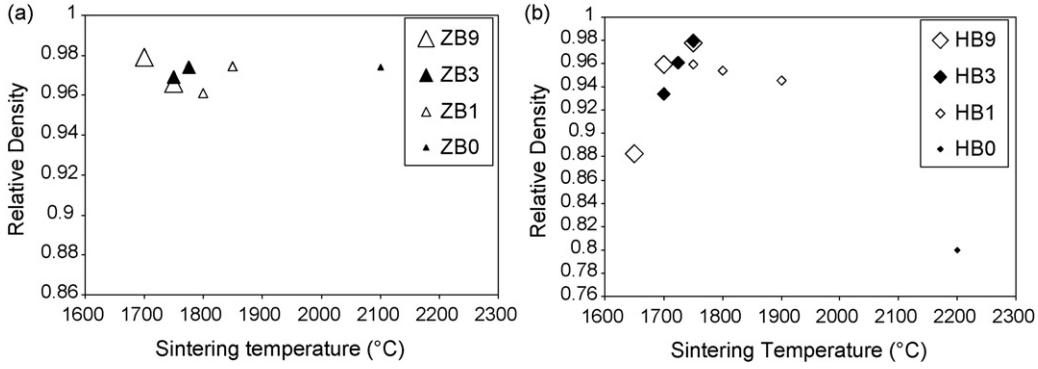

Fig. 2. Relative density data as a function of the sintering temperature for different sintering aid contents: (a) ZrB_2-based compositions and (b) HfB_2-based compositions.

Table 2
Nominal compositions, sintering parameters and volumetric amounts of extra phases calculated by image analysis, hardness and fracture toughness of relevant compositions

Sample label	Nominal composition (vol.%)	Sintering parameters[a] (°C/min/MPa)	Relative density[b] (%)	Mean grain size (μm)	SiO_2 (vol.%)	SiC (vol.%)	ZrO_2 (vol.%)	HfO_2 (vol.%)	Hardness (GPa)	Fracture toughness (MPa $m^{1/2}$)
ZB9	ZrB_2 + 9% MoSi2	1700/5/100	100	1.7 ± 0.1	3.0	1	1	–	18.2 ± 0.7	3.3 ± 0.5
ZB3	ZrB_2 + 3% $MoSi_2$	1750/3/100	100	1.9 ± 0.1	3.0	1	1	–	18.3 ± 0.6	2.6 ± 0.1
ZB1	ZrB_2 + 1% $MoSi_2$	1850/5/100	98	3.8 ± 0.2	1.5	0.5	1	–	16.5 ± 1.0	2.0 ± 0.2
ZB0	ZrB_2	2100/3/75	98	20 ± 2	–	–	–	–	15.6 ± 0.4	<2
HB9	HfB_2 + 9% $MoSi_2$	1750/3/100	100	1.0 ± 0.1	<0.5	1	–	3–4	21.2 ± 0.9	4.3 ± 0.5
HB3	HfB_2 + 3% $MoSi_2$	1750/3/100	100	0.9 ± 0.1	<0.5	1	–	3–4	22.0 ± 0.6	3.9 ± 0.4
HB1	HfB_2 + 1% $MoSi_2$	1750/3/100	99	1.0 ± 0.1	<0.5	1	–	3–4	21.1 ± 0.6	4.0 ± 0.5
HB0	HfB_2	2200/5/65	80	10 ± 1	–	–	–	–	7.0 ± 0.4	–

[a] Temperature recorded on the external wall of the graphite die.
[b] Image analysis on SEM micrographs.

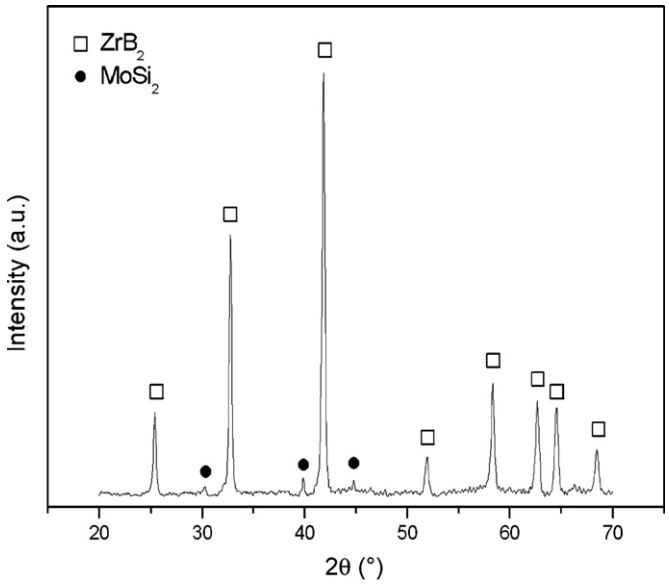

Fig. 4. X-ray diffraction spectrum of the ZrB_2 + 9$MoSi_2$ (ZB9) sintered at 1700 °C.

In the following, microstructural analysis and mechanical testing are reported for the compositions that are given in Table 2.

3.2. X-ray diffraction and microstructural features

3.2.1. ZrB_2-doped compositions

According to X-ray diffraction, the crystalline phases detected in 9% doping level compositions (ZB9) were hexagonal ZrB_2 and tetragonal $MoSi_2$ (Fig. 4). Traces of $MoSi_2$ phase were also recognizable in the diffraction spectra of the compositions with 3 vol.% doping (ZB3). In compositions with 1% $MoSi_2$ (ZB1), no diffraction peaks from $MoSi_2$ were detected.

The typical microstructures observed on fracture surfaces and polished sections of selected ZrB_2-based compositions are presented in Figs. 5 and 6a–d. The fracture surface was mainly transgranular for these composites. Black contrasting spots were identified as silica-based low-density phases. By

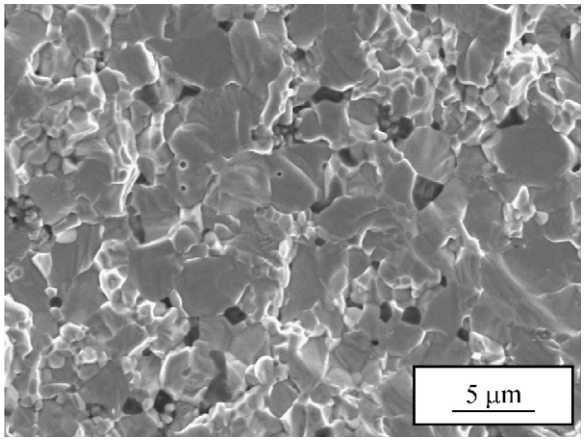

Fig. 5. Fracture surface of ZrB_2 + 3$MoSi_2$ (ZB3) sintered at 1750 °C.

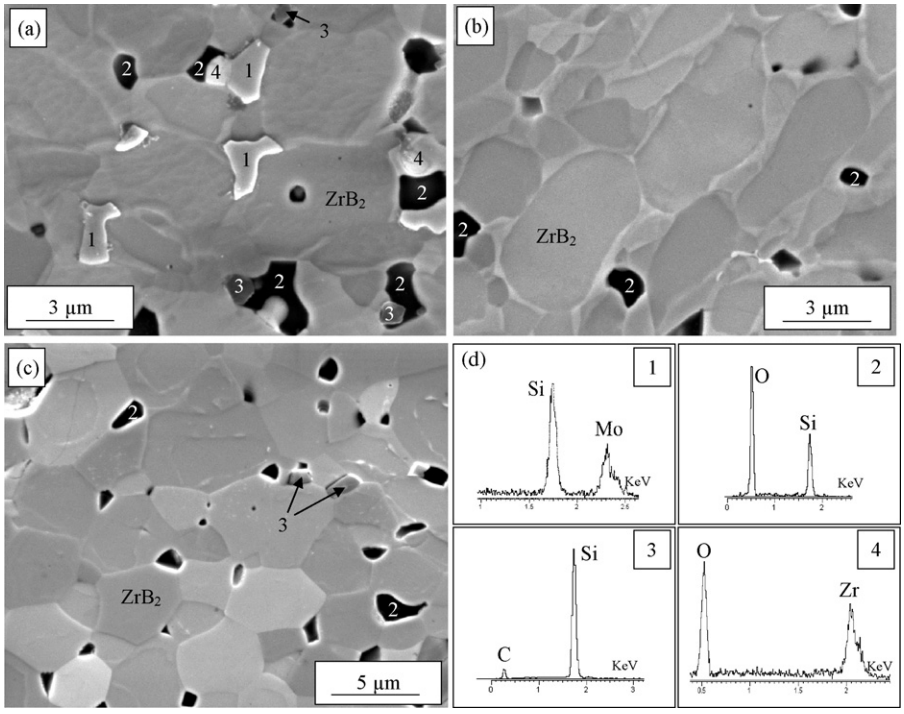

Fig. 6. ZrB_2-based compositions. Polished sections of selected samples and EDS spectra: (a) ZB9 sintered at 1700 °C, (b) ZB3 sintered at 1750 °C, (c) ZB1 sintered at 1850 °C and (d) legend: (1) $MoSi_2$, (2) SiO_2, (3) SiC and (4) ZrO_2.

SEM inspections on polished sections, no porosity was detected on ZB9 sample sintered at 1700 °C and ZB3 sample sintered at 1750 °C (Fig. 6a and b). Therefore, relative density values displayed in Fig. 2a were certainly underestimated by the presence of such low-density silica-containing phases (~3 vol.%, see Table 2) as they were neglected in the calculation of theoretical density. Silica-based phases were also frequently found to be a sink for other impurities contained in the starting powders, such as Al, N and so on. Grain coarsening and limited porosity (2%) is apparent for the composition with 1% doping (ZB1, sintering at 1850 °C), Fig. 6c. Common features for these ZrB_2-based composites were the presence of extra phases such as zirconia and SiC (see EDS spectra, Fig. 6). Zirconia could be derived both from oxygen contamination of the starting ZrB_2 powder and from the milling media. Small SiC grains were generally observed to form associated with the silica pockets, as shown in the micrograph of Fig. 6a. Their formation accounts for C contamination, due to both carbon impurities in the starting ZrB_2 powder and to the graphite-rich sintering environment, as reported below. Analysing the microstructure at lower magnitude, larger SiC agglomerates were occasionally observed in all the compositions, see an example in Fig. 7. ZrB_2 grains were found to have a sub-structure, resembling a core–shell structure, Fig. 8. By EDS analysis, carried out with reduced energy in order to limit the beam lateral spread, pure ZrB_2 phase was recognized in the cores, while Zr, B and small amounts of Mo were detected in the shell (see EDS spectrum). The latter phase was recognized as a (Zr, Mo)B_2 solid solution, in agreements with previous findings on pressureless sintered materials with addition of either Mo or $MoSi_2$.[25,26]

3.2.2. ZrB_2-monolithic material

A polished section of ZrB_2-monolithic material is displayed in Fig. 9. The material presented a very low degree of porosity in the form of closed pores evenly distributed in the microstructure. The mean grain size increased to about 20 µm. Along grain boundaries, small inclusions of BN are visible, as revealed by the EDS spectrum.

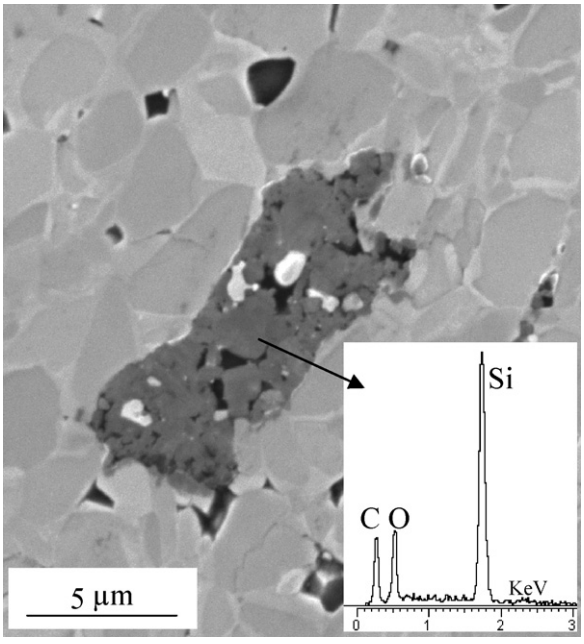

Fig. 7. Large SiC agglomerates and relative EDS spectrum showing oxygen contamination in ZB3 composition.

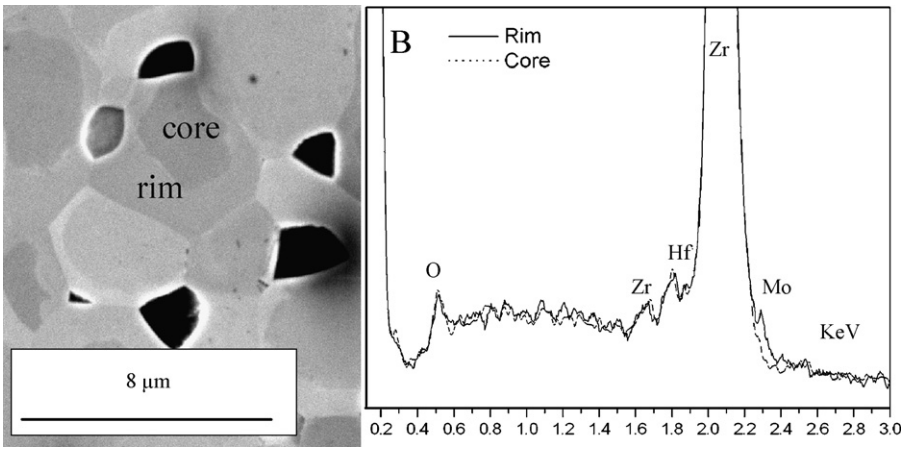

Fig. 8. Polished section of sample ZB1 sintered at 1850 °C and comparison of EDS spectra between core and rim of ZrB_2 grains.

3.2.3. *HfB_2-doped compositions*

The crystalline phases detected for compositions with 9% $MoSi_2$ (HB9) were hexagonal HfB_2 and tetragonal $MoSi_2$ (Fig. 10). However, due to the high scattering factor of the HfB_2 phase, diffraction peaks from $MoSi_2$ had very poor intensity. For lower $MoSi_2$ content, no diffraction peaks from this phase were detected. The fracture surfaces and polished sections of the compositions sintered at 1750 °C (Table 2) is presented in Fig. 11a–d. Little or no porosity was generally found in these samples, even for the lowest $MoSi_2$ content, 1%. Therefore, any discrepancy between relative density values and microstructural observations was due to formation of extra phases, neglected in the calculation of theoretical density. Fracture surfaces were mostly transgranular, Fig. 11a. Polished sections, Fig. 11 b, c and d, showed very fine microstructures, around 1 μm. The $MoSi_2$ phase had an irregular shape and, due to its ductility, was accommodated among the voids left by the diboride skeleton. Extra phases such as HfO_2, SiC and SiO_2 were observed in the microstructures (amounts reported in Table 2). The considerable amount of HfO_2 (4 vol.%) accounts for oxygen contamination of the starting powder, as reported elsewhere.[19] Agglomerates of silicon carbide particles were observed in the microstructures, see an example in Fig. 11d. The amount of SiC detected by image analysis was about 1%, in all the doped compositions (Table 2). Finally, some silica was also detected, but in considerably lower amount compared to that in the ZrB_2-based composites (~0.5%). In contrast to the ZrB_2 materials, $MoSi_2$ was found at the triple points even for HfB_2 compositions with 1% $MoSi_2$.

Sintering of HB1 at 1900 °C resulted in higher amount of porosity (5%) compared to lower temperature cycles, as reported in Section 3.1 and Fig. 2b. On the polished section of the sample (not shown), it was found that the bulk of the specimen contained pores, whilst towards the edges the microstructure was dense and on the surface, a 10 μm-thick layer of SiC was observed.

3.2.4. *HfB_2-monolithic material*

Residual porosity and grain coarsening (10 μm, see Fig. 3) are the main features which characterise the monolithic material (Fig. 12). The combination of these two features indicates that

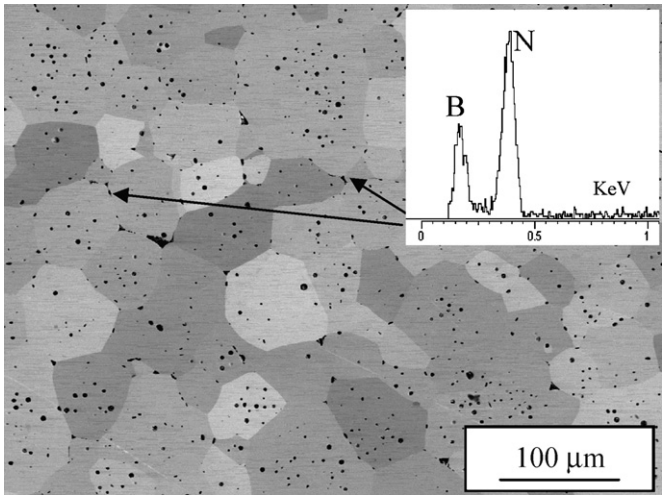

Fig. 9. Polished section of monolithic ZrB_2 sintered at 2100 °C.

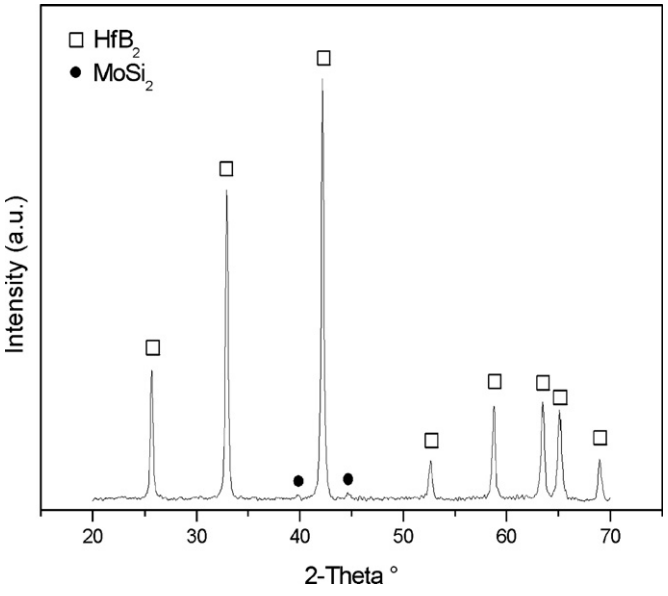

Fig. 10. X-ray diffraction spectrum of the $HfB_2 + 9MoSi_2$ (HB9) sintered at 1750 °C.

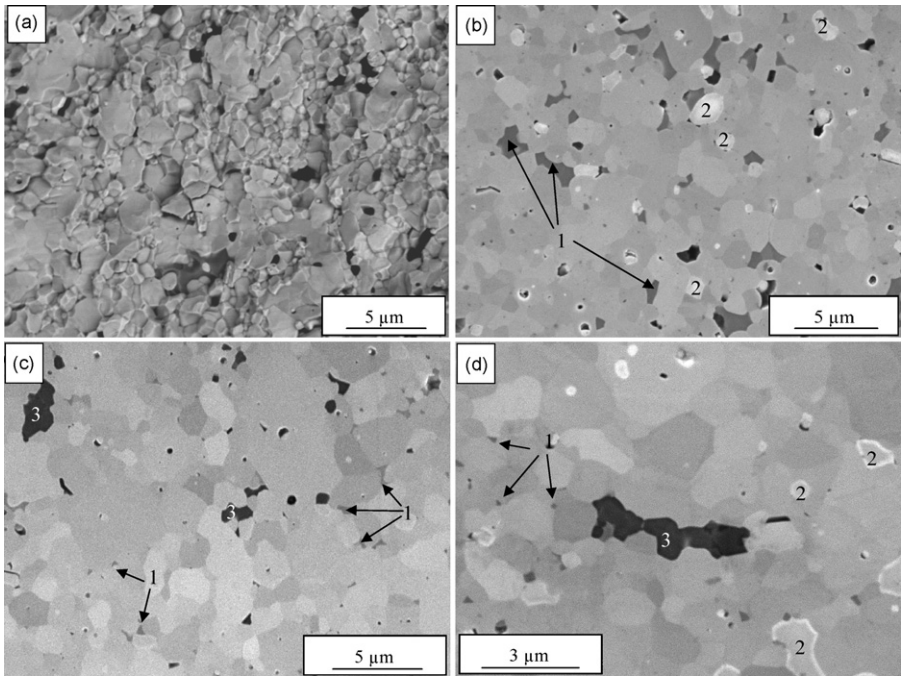

Fig. 11. HfB_2-based compositions: (a) fracture surface of $HfB_2 + 3MoSi_2$ (HB3) sintered at 1750 °C (back scattered electron imaging), (b) section of HB9 sintered 1750 °C, (c) section of HB3 sintered at 1750 °C and (d) section of HB1 sintered at 1750 °C. Legend: (1) $MoSi_2$, (2) HfO_2 and (3) SiC.

HfB_2 coarsened with poor densification, which suggests that a non-densifying vapour phase transport mechanism may be dominant at this temperature. Further tests are in progress in order to improve the final relative density.

3.3. Densification mechanisms

Density data gave evidence of the beneficial effect of $MoSi_2$ as sintering aid. Even 1 vol.% of the intermetallic compound was enough to densify both HfB_2 and ZrB_2, whilst undoped HfB_2 did not sinter even at 2300 °C. Exposure to air and the milling procedure of the starting powders for prolonged times is known to cause oxygen take up. For metal diborides (MB_2), the contamination of oxygen was proposed to be a combination of metal oxide and boron oxide.[27] Since the presence of surface oxides such as B_2O_3 and Hf-/Zr-O_2 is generally considered very detrimental for the sintering of these borides, the addition of $MoSi_2$ must have been effective in removing oxygen bearing species from the MB_2 particle surfaces. In addition, it has been reported that field assisted sintering techniques can also cause removal of oxide species from particle surface, through different mechanisms such as resistance heating and/or thermal and electrical breakdown.[4,5] However, before discussing possible reactions that might take place during the sintering process, one has to keep in mind that the actual temperature inside the specimens is significantly higher than that recorded on the surface of the die.[8,19] The temperature mismatch depends on many factors such as the size of the die, the quality of vacuum, the level of insulation of the die, thermal and electrical conductivity of the die, etc. The dies used in this work have an outer diameter of 3 cm and a height of 3 cm and a double layer of graphite blanket were placed around the die (in total 1 cm insulation) in order to minimize the heat loss. Under this conditions we could estimate the temperature mismatch to be around 100–125 °C up to 1700 °C. Alumina, which melts around 2070 °C, could be sintered at 1850 °C without any feature of being melted, suggesting that the temperature mismatch at this temperature is ≤200 °C. However, the mismatch increases with increasing the temperature and it is likely that in the 1900–2200 °C range it might be around 250°. Accordingly, when the recorded temperature was ≤1800 °C, then the temperature that the specimens experienced ought to be lower than the melting temperature of $MoSi_2$ (2020 °C[28]) and when the temperature recorded by the optical pyrometer was >1850 °C, sintering very likely occurred at a temperature close or even higher than the melting temperature of $MoSi_2$. The HB1 composition sintered at 1900 °C contained a higher amount of porosity (5%) compared to lower temperature

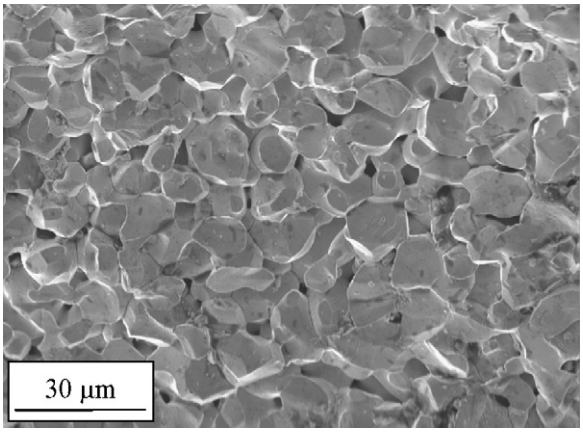

Fig. 12. Fracture surface of monolithic HfB_2 sintered at 2200 °C.

cycles, as previously mentioned. According to microstructural observations, it is likely that $MoSi_2$ melted at this temperature and was rapidly squeezed out. The fast depletion of the sintering aid was hence detrimental for the densification.

The following considerations concern sintering temperatures was in the range of 1750–1850 °C, i.e. lower than the melting point of $MoSi_2$. The formation of secondary species such as SiO_2 and SiC detected after sintering was used to track back the interactions between $MoSi_2$, oxygen bearing species (B_2O_3) and carbon provided by the sintering environment (mould, dies). Considering that the activity of C is very high in this temperature range, the following reactions can be hypothesized:

$$2MoSi_2 + 2B_2O_3 + C = 2MoB_2 + 3SiO_2 + 1SiC \quad (1)$$

$$2MoSi_2 + B_2O_3 + 2.5\,C = 2MoB + 1.5SiO_2 + 2.5SiC \quad (2)$$

According to thermodynamic calculations[29], these reactions are energetically favoured at the sintering conditions employed ($\Delta G < 0$). It should be noted that silica is liquid at temperature >1725 °C, which could explain liquid ejection observed during sintering of compositions with 9% $MoSi_2$. Reactions 1–2 suggest that, depending on the local chemistry, i.e. the degree of oxygen contamination, the amount of $MoSi_2$ added and the C availability, different reaction products may be formed. A commercial software program[29] was used to simulate chemical reactions occurring during the sintering cycle at 1850 °C, ambient pressure, introducing fixed amounts of carbon and B_2O_3 as reagents and varying the $MoSi_2$ content between 0 and 3 kmol. The products which are thermodymically favoured to form are SiO_2, SiC and Mo-B species and are displayed in the diagrams of Fig. 13 representing the cases: amount of B_2O_3 > amount of C (Fig. 13a) and *vice versa* (Fig. 13b). The occurrence of the proposed reactions was partially supported by the SEM–EDS studies. In ZrB_2-based materials, silica formation was quite abundant in comparison with SiC and the starting amount of $MoSi_2$ was considerably reduced after sintering. The equilibrium composition of the products is therefore similar to that proposed by Fig. 13a. Actually, we did not observed any Mo-B species as predicted by the reactions 1,2 and the calculations (Fig. 13a) but the formation of (Zr, Mo)B_2 solid solutions. The database of the thermodynamic calculation program did not contain any data for (Zr, Mo)B_2 solid solutions implying that the calculations do not exclude that (Zr, Mo)B_2 species might be formed in our case instead of the predicted Mo-B ones. Conversely, in HfB_2-based composites, SiC production was more abundant than silica formation (see Table 2) and $MoSi_2$ starting amount was only partially consumed during sintering. According to the SEM resolution, no solid solutions were detected for HfB_2. In this case, the equilibrium composition of the products was closer to the diagram of Fig. 13b.

Although the above calculations are certainly an oversimplification of the chemistry of these systems, nevertheless they suggest that for UHTC samples doped with $MoSi_2$, densification was mainly activated by chemical mechanisms involving the sintering aid and surface oxides with consequent removal of surface oxides from MB_2 particles surface and formation of liquid phases. These phenomena were further enhanced by application

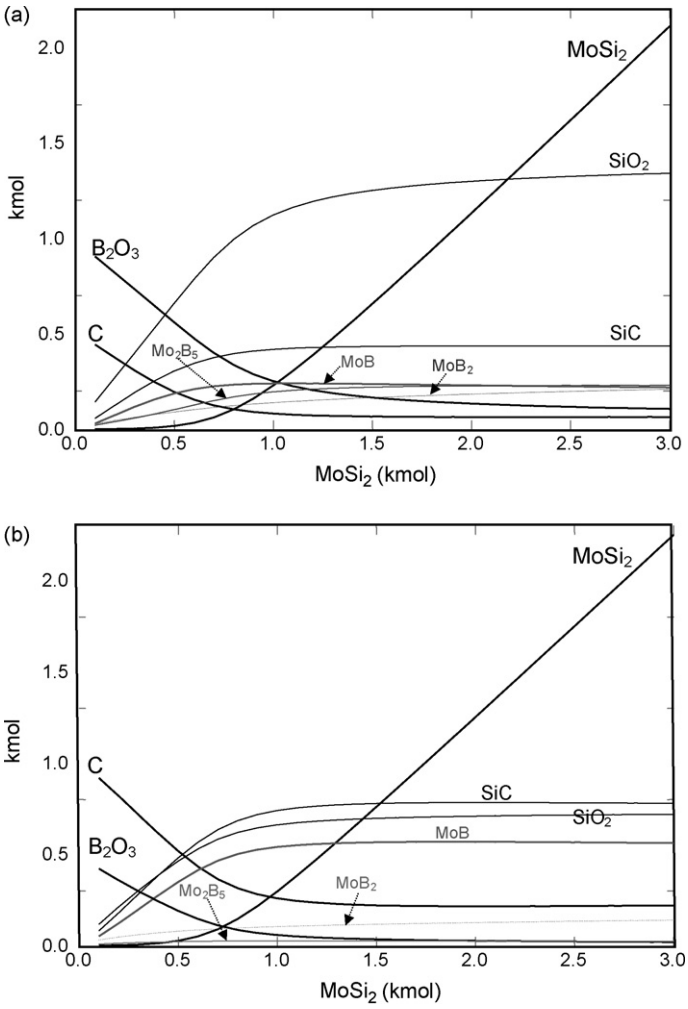

Fig. 13. Stable reaction products calculated at 1850 °C, ambient pressure, for increasing $MoSi_2$ content. (a) Reagents starting amount: $C = 0.5$ kmol, $B_2O_3 = 1$ kmol and (b) reagents starting amount: $C = 1$ kmol, $B_2O_3 = 0.5$ kmol.

of the external electrical field which allowed full densification in very short times compared to other conventional techniques.

The densification of undoped ZrB_2 powder occurred through solid-state sintering mechanisms. Rapid heating rates and electrical discharge helped removal of surface B_2O_3. However, the concurrent action of chemical phenomena cannot be ruled out. The observed formation of small amounts of BN in the microstructure, suggests that B_2O_3 removal could have occurred also through the following reaction:

$$B_2O_3 + 2N + 3C = 2BN + 3CO(g) \quad (3)$$

which has a negative free Gibbs energy.[29] In this reaction, N is an impurity of the starting ZrB_2 powder and C is provided by the graphite-rich sintering environment. Finally, causes for the low-density results obtained for HfB_2 monolithic materials are still under investigation.

3.4. Mechanical properties

Preliminary hardness and toughness tests were carried out on selected compositions as shown in Table 2. The results dis-

played revealed that, irrespective of the $MoSi_2$ content, ZB3 and ZB9 had the same value of hardness as well as the HB1, 3 and 9 samples. Both ZrB_2-based compositions (with the exception of ZB1) and HfB_2-based compositions had similar values of mean grain size and density which are the most important factors affecting the hardness. HfB_2-based compositions were harder than corresponding ZrB_2-ones, due to their finer microstructure. On the other hand, the hardness decrease observed for ZB0, ZB1 and HB0 is due to grain coarsening and/or porosity.

Concerning the fracture toughness, HfB_2 compositions are insensitive to change of $MoSi_2$ amount between 1 and 9%. For ZrB_2-compositions there is an approximately linear decrease with decreasing the amount of $MoSi_2$. This feature seems to indicate that $MoSi_2$ acted as reinforcing phase for ZrB_2, even if the toughening mechanisms exerted by this phase are not known. Due to its high thermal expansion coefficient ($8.5–9 \times 10^{-6}\,^{\circ}C^{-1}$)[30], $MoSi_2$ should generate compressive residual stress in ZrB_2 ($6–7 \times 10^{-6}\,^{\circ}C^{-1}$)[30] phase. However, SiC ($4.5 \times 10^{-6}\,^{\circ}C^{-1}$)[30] and SiO_2 ($0.5 \times 10^{-6}\,^{\circ}C^{-1}$)[30] phases should generate tensile stresses in ZrB_2, by virtue of their low thermal expansion coefficients. Therefore, decrease of $MoSi_2$ content and concurrent increase of SiO_2/SiC species could be responsible for the weakening of the microstructure.

4. Conclusions

ZrB_2- and HfB_2-based composites containing 1, 3, and 9 vol.% $MoSi_2$, respectively, were fully densified by spark plasma sintering at temperatures ranging from 1700 to 1950 °C, using a heating rate of 100 °C/min and an applied pressure of 100 MPa. Densification was presumed to occur through removal of surface oxides from the boride particles and formation of liquid phases. Sintering mechanisms were enhanced by application of the electric field which allowed full densification in very short times and with very low content of sintering aid compared to conventional techniques.

Attempts were also made to densify ZrB_2 and HfB_2 with no sintering aid. ZrB_2 was finally densified to 98%, however a notable coarsening of the microstructure occurred (20 μm). Eighty percentages of relative density was instead of the maximum value obtained for HfB_2.

For dense materials, hardness and fracture toughness values were in the range of 17–22 GPa and of 2.6–4 MPa $m^{1/2}$, respectively.

References

1. Shen, Z., Zhao, Z., Peng, H. and Nygren, M., Formation of tough interlocking microstructures in silicon nitride ceramics by dynamic ripening. *Nature*, 2002, **417**, 266–269.
2. Munir, Z. A., Anselmi-Tamburini, U. and Ohyanagi, M., The effect of electric field and pressure on the synthesis and consolidation of materials. *J. Mater. Sci.*, 2006, **41**, 763–777.
3. Nygren, M. and Shen, Z., Novel assemblies via spark plasma sintering. *Sil. Ind.*, 2004, **69**, 211–218.
4. Groza, J. R. and Zavaliangos, A., Sintering activation by external electrical field. *Mater. Sci. Eng.*, 2000, **A287**, 171–177.
5. Groza, J. R., Garcia, M. and Schneider, J. A., Surface effects in field assisted sintering. *J. Mater. Res.*, 2001, **16**, 286–292.
6. Gao, L., Shen, Z., Myamoto, H. and Nygren, M., Superfast densification of oxide/oxide ceramic composites. *J. Am. Ceram. Soc.*, 1999, **82**, 1061–1063.
7. Perera, D. S., Tokita, M. and Moricca, S., Comparative study of fabrication of Si_3N_4/SiC composites by spark plasma sintering and hot isostatic pressing. *J. Eur. Ceram. Soc.*, 1998, **18**, 2757–2767.
8. Anselmi-Tamburini, U., Gennari, S., Garay, J. E. and Munir, Z. A., Fundamental investigations on the spark plasma sintering/synthesis process. II. Modelling of current and temperature distributions. *Mater. Sci. Eng. A*, 2005, **394**, 139–148.
9. Opeka, M. M., Talmy, I. G. and Zaykoski, J. A., Oxidation-based materials selection for 2000 °C + hypersonic aerosurfaces: theoretical consideration and historical experience. *J. Mater. Sci.*, 2004, **39**, 5887–5904.
10. Upadhya, K., Yang, J. M. and Hoffmann, W. P., Materials for ultrahigh temperature structural applications. *Am. Ceram. Soc. Bull.*, 1997, **58**, 51–56.
11. Van de Goor, G., Sagesser, P. and Berroth, K., In *Electrically Conductive Ceramic Composites in Advanced Multilayered and Fibre-Reinforced Composites*, ed. Y. M. Haddad. Kluwer Academic Pub, The Netherlands, 1998, pp. 311–322.
12. Clougherty, E. V., Kalishi, D. and Peters, E. T., Research and development of refractory oxidation resistant diborides, AFML-TR-68-190, 1968.
13. Gasch, M., Elleby, D., Irby, E. I., Beckam, S., Gusman, M. and Johnson, S., Processing, properties and arc jet oxidation of hafnium diboride/silicon carbide ultra high temperature ceramics. *J. Mater. Sci.*, 2004, **39**, 5925–5937.
14. Opeka, M. M., Talmy, I. G., Wuchina, E. J., Zaykoski, J. A. and Cause, S. J., Mechanical, thermal, and oxidation properties of refractory hafnium and zirconium compounds. *J. Eur. Ceram. Soc.*, 1999, **19**, 2405–2414.
15. Wuchina, E., Opeka, M., Causey, S., Buesking, K., Spain, J., Cull, A., Routbort, J. and Guitierrez-Mora, F., Designing for ultrahigh-temperature applications: the mechanical and thermal properties of HfB_2, HfC_x, HfN_x, and alpha Hf(N). *J. Mater. Sci.*, 2004, **39**, 5939–5949.
16. Chamberlain, A. L., Fahrenholtz, W. G., Hilmas, G. E. and Ellerby, D. T., High-strength zirconium diboride-based ceramics. *J. Am. Ceram. Soc.*, 2004, **87**, 1170–1172.
17. Chamberlain, A. L., Fahrenholtz, W. G. and Hilmas, G. E., Pressureless sintering of zirconium diboride. *J. Am. Ceram. Soc.*, 2006, **89**, 450–456.
18. Telle, R., Sigl, L. S. and Takagi, K., Boride-based hard materials. In *Handbook of ceramic hard materiali*, *vol. 2*, ed. R. Riedel. Wiley–VCH, Weinheim, 2000, pp. 802–945.
19. Anselmi-Tamburini, U., Kodera, Y., Gasch, M., Unuvar, C., Munir, Z. A., Ohyanagi, M. and Johnson, S. M., Synthesis and characterization of dense ultra-high-temperature thermal protection materials produced by field activation through spark plasma sintering (SPS). I. Hafnium diboride. *J. Mater. Sci.*, 2006, **41**, 3097–3104.
20. Sciti, D., Monteverde, F., Guicciardi, S., Pezzotti, G. and Bellosi, A., Microstructure and mechanical properties of ZrB_2- and $MoSi_2$-ceramic composites produced by different sintering techniques. *Mater. Sci. Eng. A*, 2006, **434**, 303–309.
21. Sciti, D., Silvestroni, L. and Bellosi, A., Fabrication and properties of HfB_2–$MoSi_2$ composites produced by hot pressing and spark plasma sintering. *J. Mater. Res.*, 2006, **21**, 1460–1466.
22. Monteverde, F. and Bellosi, A., On the comparison of additive-free HfB2-SiC ceramics sintered by reactive hot pressing and spark plasma sintering. In *Ceramic engineering and science Proceedings of the 28th international conference on advanced ceramics and composites, vol. 25, no. 4*, 2004.
23. Sciti, D., Brach, M. and Bellosi, A., Oxidation behaviour of a pressureless sintered ZrB_2–$MoSi_2$ ceramic composite. *J. Mater. Res.*, 2005, **20**, 922–930.
24. Evans, A. G. and Charles, E. A., Fracture toughness determinations by indentation. *J. Am. Soc.*, 1976, **59**, 371–372.
25. Yan, Y., Huang, Z., Dong, S. and Jiang, D., Pressureless sintering of high-density ZrB_2–SiC ceramic composites. *J. Am. Ceram. Soc.*, 2006, **89**, 3589–3593.
26. Silvestroni, L. and Sciti, D., Effects of $MoSi_2$ additions on the properties of (Hf- and Zr-)B_2 composites produced by pressureless sintering. *Scripta Mater.*, 2007, **57**, 165–168.

27. Øvrebo, D. N. and Riley, F. L., In *Conference and Exhibition of the sixth ECERS, Extended Abstracts, British Ceramic Proceedings 60, vol. 2*, 1999, pp. 787–803.
28. Jeng, Y.-L. and Lavernia, E. J., Review, processing of molybdenum disilicide. *J. Mater. Sci.*, 1994, **29**, 2557–2571.
29. *HSC Chemistry for Windows 6.0*, Outokumpu Research OY, Pori, Finland, 2006.
30. Shackelford, J. F. and Alexander, W., ed., *CRC Materials Science and Engineering Handbook*. 3rd ed. CRC Press, Boca Raton Fl, 2001, pp. 449–482.